12th INTERNATIONAL SCIENTIFIC CONFERENCE ON DEFENSIVE TECHNOLOGIES
OTEH 2026
Serbia, Tara, 21 - 24 October 2026

DIFFERENT SYNTHETIC ROUTES OF CERIUM-DIOXIDE NANOPARTICLES PREPARATION AND THEIR EFFICIENCY IN SULFUR MUSTARD REMOVAL

MAJA VITOROVIĆ-TODOROVIĆ
Military Technical Institute, Belgrade, majavitod@gmail.com

ALEKSANDAR ĆITIĆ
Military Technical Institute, Belgrade, woteusrb@gmail.com

Abstract: *Highly toxic compounds such as chemical warfare agents (CWAs) are subject to strict international control, and their use is limited to protective and research purposes under national and international legislation, most notably the Chemical Weapons Convention. However, the potential use of these agents by terrorist groups, as well as their accidental release, continues to pose a serious threat to civilian populations. Ongoing efforts are focused on developing new strategies and technologies for the removal, decontamination, and detoxification of CWAs. One promising approach involves the use of metal oxide nanoparticles for the catalytic degradation of CWAs, such as magnesium oxide, titanium dioxide, and zirconium hydroxide being the most extensively studied materials. More recently, cerium dioxide (CeO_2) nanoparticles have demonstrated considerable potential for CWAs degradation, due to their ability to readily switch between +3 and +4 oxidation states. The degradation efficiency of CeO_2 nanoparticles strongly depends on their morphology, aggregation state, and surface area. In this study, we explored several synthetic routes for CeO_2 nanoparticles preparation, including homogeneous hydrolysis, the oxalate route, precipitation with ammonium-carbonate and the solution combustion synthesis. The morphology and structure of the obtained particles were characterized using scanning electron microscopy (SEM), Raman spectroscopy and N_2 adsorption experiments. Their degradation efficiency toward HD was evaluated by gas chromatography–mass spectrometry. In most cases, CeO_2 nanoparticles exhibited highly efficient removal of HD agent.*

Keywords: *cerium-dioxide, nanoparticles, catalytic degradation, chemical warfare agents*

1. INTRODUCTION

Chemical warfare agents (CWAs) belong to a group of exceptionally hazardous toxic chemicals whose production, possession and use are rigorously regulated by national legislation and international agreements, particularly the Chemical Weapons Convention. Although their legitimate handling is restricted to defensive, analytical and research activities, the risk associated with their intentional deployment in armed conflicts or terrorist attacks has not been eliminated. In addition, accidental releases during storage, transport or handling may also result in severe consequences for both human health and the environment. These concerns have stimulated continued research into advanced decontamination approaches, including more effective reactive formulations, improved detoxification technologies and the design of novel materials for individual and collective protection. In this sense, nanotechnologies, particularly the utilization of catalytically active metal-oxide nanoparticles as carriers of active chemistry represent a good starting point for the development of various decontamination formulations and novel protective materials. Stoichiometric nanocrystalline MgO was one of the first oxides proposed for the destruction of CWA [1], followed by other types of nanoparticles, including calcium-oxide (CaO) [2], titanium-dioxide (TiO_2) [3] and zirconium(IV)-hydroxide ($Zr(OH)_4$)[4]. While earth-alkaline oxides and $Zr(OH)_4$ decompose organophosphate agents *via* hydrolytic pathways, TiO_2 degrade organic substances by free-radical mechanism generated with water as an intermediate reagent in decomposition reactions. Here should be emphasized that not all CWAs are equally resistant toward degradation. For instance, G-class organophosphate agents namely soman (3,3-dimethylbutanyl methylphosphonofluoridate, GD) and sarin (2-propanyl methylphosphonofluoridate, GB) easily degrade by changing pH of the environment with the half-time of reaction being only 2 minutes in the pH above 8 and below 4. For detoxification of these agents, only hydrolytic cleavage of P-F bond is needed (Figure 1). On the contrary, some other types of agents are more resistant toward decontamination, and require both oxidative and hydrolytic degradation pathways. These are blister agent, sulfur mustard (1-chloro-2-[(2-chloroethyl)-sulfanyl]-ethane, HD) and VX (S-{2-[di(propan-2-yl)amino]ethyl} O-ethyl methylphosphonothioate). Degradation pathways of these two agents should be strictly controlled since there is a possibility of occurrence of byproducts which retain their toxic properties.

Corresponding author: M. Vitorović-Todorović
E-mail: majavitod@gmail.com
DOI: 10.5937/OTEH26129V

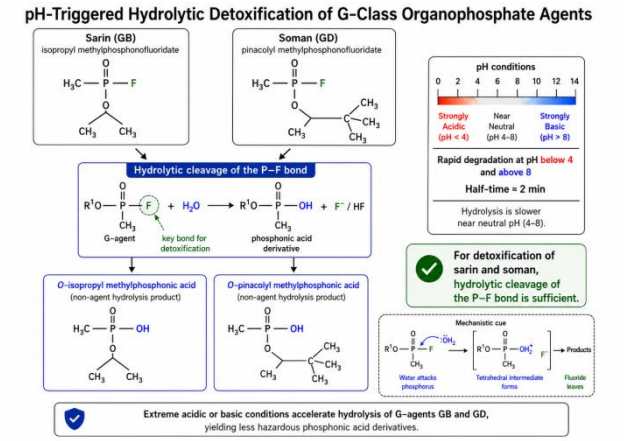


Figure 1. Hydrolytic detoxification of G-agents.

For instance, the partial oxidation pathway of sulfur mustard should be strictly controlled to yield sulfoxide product only, since further oxidation to sulfone gives product with blistering properties (Figure 2) [5].

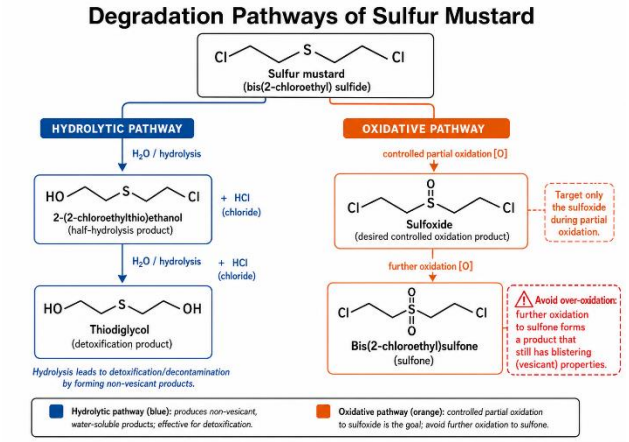


Figure 2. Degradation pathways of sulfur mustard.

The hydrolytic pathways of VX should be also strictly selective in a way that yield product of P-S bond cleavage only. If the P-O bond is cleaved, a very toxic EA2192 product, with potent anticholinesterase activity is obtained [6]. Moreover, further oxidation of diisopropylethylthio moiety is desirable (Figure 3).

Based on all of these stated above, there is a need for efficient decontamination agent which may provide both oxidative and hydrolytic pathways of CWA degradation. In this sense, nanoparticles of cerium-dioxide (CeO_2) seemed as a promising agent due to the several interesting properties. Cerium is the first element of lanthanide series. Its 4f orbitals are shielded by 5p and 4d orbitals, the electronic configuration of Ce+3 ion is $[Xe]4f^1$. By losing 3 electrons to achieve a +3 oxidation state, it gives up the two 6s and one 5d electron leaving only one 4f electron.

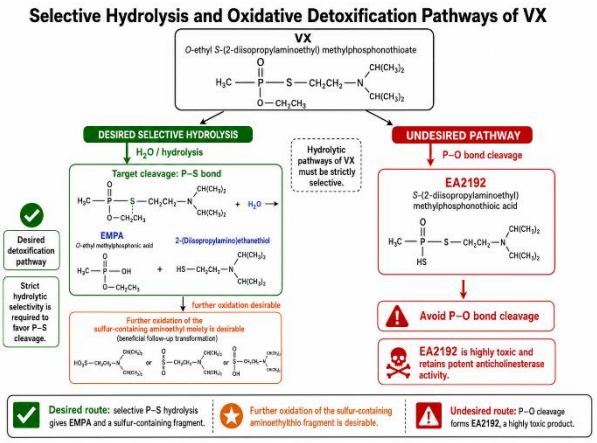


Figure 3. Degradation pathways of VX.

Due to an interesting electronic configuration, Ce exists easily in 3+ and 4+ oxidation states, meaning that $CeO_2 \rightarrow Ce_2O_3$ transition easily takes place, especially if the material is in its nano-form. Therefore, nanoceria has significant capacity to store and release oxygen and repeatedly pass through redox cycles rapidly. Due to these particular properties, CeO_2 nanoparticles are widely used as fuel oxidation catalyst [7], automotive exhaust treatment [8] and also these nanoparticles may exhibit enzyme mimicking activities including superoxide-dismutase, catalase, and phosphatase enzymes [9], [10].

The degradation efficacy of CeO_2 nanoparticles is strongly dependent upon their crystallite size, presence of oxygen vacancies and the presence of crystal lattice defects as well as their morphology. On the other hand, all these properties depend upon the synthetic routes used to obtain CeO_2 nanoparticles. In this study, we examined the influence of the synthetic routes for CeO_2 on their morphology and degradation efficacy using sulfur mustard. The aim of this work was to decipher whether degradation efficacy may be finely tuned by the synthetic routes used to obtain CeO_2 nanoparticles and how their morphology is related to their catalytic activity. For the synthetic routes we have chosen the most employed and the best described in the scientific literature, including: homogenous hydrolysis, precipitation with oxalic acid, precipitation with ammonium-bicarbonate and solution combustion synthesis, using urea as a fuel. Together with commercially available CeO_2 nanoparticles (25 nm in size, Sigma Aldrich) amorphous and the same that is annealed at 500 °C to induce crystallization. This yielded totally six different CeO_2 nanoparticles samples (Table 1).

The morphology and structure of the obtained particles were characterized using scanning electron microscopy (SEM), Raman spectroscopy and N_2 adsorption (BET isotherm analysis). Their degradation efficiency toward HD was evaluated by gas chromatography–mass spectrometry.

Table 1. CeO_2 nanoparticle samples investigated in this work.

Sample code	Synthetic route / origin	Key reagent or treatment	Brief description
CeO_2-1	Homogenous hydrolysis	Urea	CeO_2 nanoparticles obtained by homogeneous hydrolysis
CeO_2-2	Precipitation	Oxalic acid	CeO_2 nanoparticles obtained via oxalate precipitation route
CeO_2-3	Precipitation	Ammonium bicarbonate	CeO_2 nanoparticles obtained by carbonate/bicarbonate precipitation
CeO_2-4	Solution combustion synthesis	Urea as fuel	CeO_2 nanoparticles synthesized by solution combustion route
CeO_2-5	Annealed commercial CeO_2	Annealed at 500°C	Commercial CeO_2 nanoparticles, annealed at 500°C
CeO_2-6	Commercial CeO_2	Sigma-Aldrich, 25 nm	Commercial CeO_2 nanoparticles

2. MATERIALS AND METHODS

All chemicals used in this work were purchased from Merck or Sigma Aldrich and were used without further purification. The HD agent was synthesized at Military Technical Institute, Belgrade and its purity was checked by the GC/MS system, confirming at least 95% of purity.

Caution: *Chemical warfare agents are highly toxic and strictly regulated substances. All CWA-related experiments were conducted solely for the research purposes in an authorized facility by trained personnel, following approved safety, containment, decontamination, and waste-disposal procedures, in compliance with institutional, national, and Chemical Weapons Convention requirements. Unauthorized handling or use of these substances must not be attempted.*

2.1. CeO_2 nanoparticles preparation

Homogenous hydrolysis

The 3 g (6.91 mmol) of $Ce(NO_3)_3x6H_2O$ were placed in the 50 mL beaker and dissolved in 10 mL of hot deionised water with the addition of 1,5 mL of concentrated nitric acid. This solution was transferred into 1L round bottom 2- or 3-necked flask equipped with a magnetic stirrer and a reflux condenser. This solution was diluted with the 400 mL of deionised water, and 50 g of urea was added divided in ten smaller portions with stirring applied. After that, the mixture was heated at 90°C, to induce slow and steady decomposition of urea and consequent increase in pH of the solution, which causes white precipitate of $Ce(OH)_4$ to occur. After cooling the mixture to room temperature, the precipitate was separated by filtration and dried in the atmosphere at 105 °C. The $Ce(OH)_4$ obtained was further calcined at 500 °C for 2 hours to induce dehydration and crystallization of the CeO_2. This sample was designated as CeO_2_1.

Oxalate precipitation

The 8,6 g (19,8 mmol) $Ce(NO_3)_3x6H_2O$ were fully dissolved in 100 mL of deionized water, in 250 mL laboratory beaker that was placed on the magnetic stirrer. The 3 g of oxalic acid (23,88 mmol) was fully dissolved in the minimal amount of deionized water. This solution was transferred into dropping funnel and slowly, during 3h was added drop wise into solution of cerium-nitrate under vigorous stirring. The white precipitate of cerium(III)-oxalate is formed. The stirring of the mixture was continued for additional hour after the addition of oxalic acid. After that, the white precipitate was separated by filtration, and dried in the oven at 105 °C. The cerium-oxalate obtained was further calcined at 500 °C for 2 hours to induce combustion of the organic residue and crystallization of the CeO_2. This sample was designated as CeO_2_2.

Precipitation with ammonium-carbonate

The 8,6 g (19,8 mmol) $Ce(NO_3)_3x6H_2O$ were fully dissolved in 100 mL of deionized water, in 250 mL laboratory beaker that was placed on the magnetic stirrer. The 4,8 g of ammonium-carbonate (50,00 mmol) is fully dissolved in 100 mL of deionized water. This solution was transferred into dropping funnel and slowly, during 3h was added dropwise into the solution of cerium-nitrate under vigorous stirring. The white precipitate of cerium(III)-carbonate is formed. The stirring of the mixture was continued for additional hour after the addition of ammonium-carbonate. After that, the white precipitate was separated by filtration, and dried in the oven at 105 °C. The cerium-carbonate obtained was further calcined at 500 °C for 2 hours to induce combustion of the organic residue and crystallization of the CeO_2. This sample was designated as CeO_2_3.

The solution combustion synthesis

The stoichiometric fuel-to-oxidizer ratio was calculated according to the total oxidizing and reducing valences of the reactants, following the propellant chemistry approach. Considering urea as fuel with a reducing valence of +6 and cerium nitrate as an oxidizer with an effective oxidizing valence of −14 for CeO_2 formation, the stoichiometric molar ratio $Ce(NO_3)_3 \cdot 6H_2O$: urea was 1 : 7/3. Therefore, 4,3 g (9,9 mmol) of $Ce(NO_3)_3x6H_2O$ and 1,39 g (23.1 mmol) were dissolved in 30 mL of deionized water in a 250 mL beaker with vigorous stirring. After the full dissolution of the compounds, the mixture was heated slowly to evaporate a portion of water and to form a viscous gel. When the gel is being formed, the temperature of the heater was increased to 450 °C to induce combustion of the mixture. After combustion, the dry pale yellow CeO_2 is formed in the beaker. The cerium-dioxide obtained was further calcined at 500 °C for 2 hours to induce crystallization. This sample was designated as CeO_2_4.

Two other samples were: commercially available calcined at 500 °C was designated as CeO_2_5, and commercially available, amorphous without any thermal treatment was designated as CeO_2_6.

2.2. Morphological characterisation of the samples

The morphology and the size of the nanoparticles were investigated by scanning electron microscopy using JEOL

JSM-660 LV microscope. The surface of the samples was covered with layer of graphite to assure conductivity. The EDS analysis was done by energy dispersive spectrometer EDS OXFORDX-Max with Aztec software.

The Raman spectra of the samples CeO_2_2 and CeO_2_6 were recorded on Anton Paar Cora 5001 spectrometer. The BET surface areas for the samples CeO_2_3, CeO_2_5 and CeO_2_6 were determined by N_2 adsorption experiments using Anton Paar Nova 600 BET analyser.

2.3. HD degradation experiments

For the HD degradation experiments, the 30 mg of the each CeO_2 sample was placed in each of the eight eppendorf 2 mL microtubes. The solution of the HD of concentration 10 mg/mL was prepared in the *n*-hexane. The 50 μL of the HD solution was pipetted in shortest possible time interval in all test tubes. In the first tube, 950 μL of isopropanol was added immediately to terminate the degradation reaction (that is visibile almost as zero point time on the graph, while it is actually 20-30 seconds). After that, in the time intervals of 10, 20, 30, 40, 50, 60 and 70 min the isopropanol was added in test vials. The extraction of the remaining HD and possible degradation products was done by shaking the tubes for 15 minutes, and then the solid was separated by centrifugation at 12000 rpm. The 10 μL aliquot was drawn from the supernatant and placed in GC-MS vials filled with 980 μL of acetonitrile and 10 μL of the internal standard solution, naphthalene-d_8. The amount of HD was quantified and the resulted chromatogram inspected for the presence of degradation products. Calibration standards and the samples were analyzed on Shimadzu GC-MS QP2020 instrument, and the peak area in the chromatogram and the creation of the calibration curve (peak area vs. concentration) was done using Shimadzu LabSolution software. For the quantification of HD, the characteristic and the most intensive mass ion m/z 109 was used. The experimental conditions for the GC-MS instrument are given in the Table 2.

Table 2. GC-MS conditions

GC Conditions	
Parameter	**Value**
Starting column temperature	40 °C, 3 min
Temperature program	40-150°C, 10°C/min, 150-280 °C, 25°C/min, 280 °C, 10,8 min
Injector temperature	250 °C
Injection type	Grob type. Splitles t 0,75 min
Colum type	DB-5
Column dimensions	30 m x 0,25 mm ID x 0,25 μm
Carrier gas	Helium, 32 cm/sec
MS Conditions	
Parameter	**Value**
Temperature transfer line	280 °C
Temperature ion source	230 °C
Temperature detector	150 °C
Electron energy	70 eV
Mass range	35-500 *m/z*
Scanning rate	3,15 scan/sec
Library	NIST 05 Mass Spectral Data Base

3. RESULTS AND DISCUSSION

3.1. CeO_2 nanoparticles preparation

The all four synthetic procedures were easily reproduced, and the CeO_2 was obtained in relatively high yields. The differences between appearance of the crystallites for the different samples was obvious even with a naked eye. For instance, the samples obtained with precipitation by oxalic acid or ammonium-carbonate, CeO_2_2 and CeO_2_3 were very light and highly voluminous, while the sample obtained by solution combustion synthesis, CeO_2_4 was heavy, firm and appear more aggregated than the rest of the samples.

3.2. Morphology of the CeO_2 nanoparticles

The SEM images of all samples in two different magnifications are given in Figures 4 and 5.

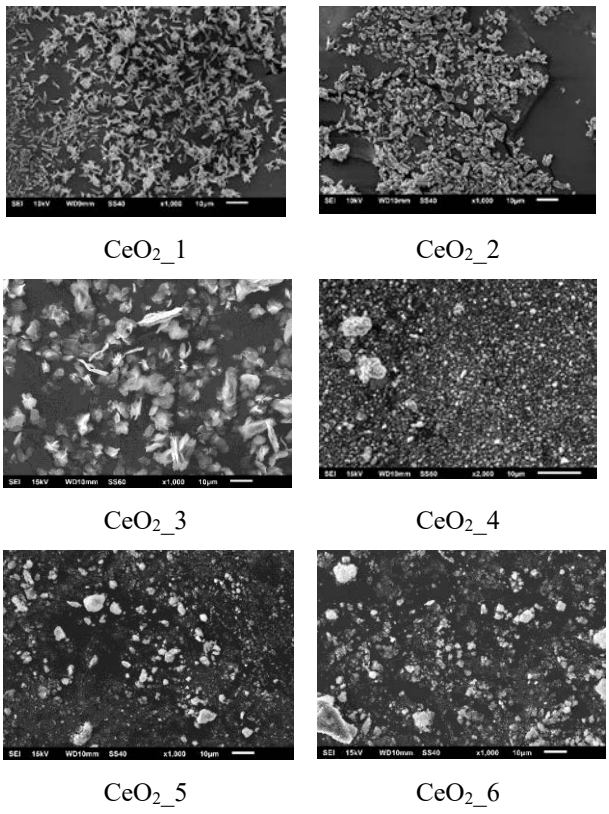


Figure 4. The SEM images of the CeO_2 samples under magnification of 1000x.

SEM analysis revealed pronounced morphology differences among the CeO_2 samples obtained by different synthetic routes. CeO_2_1, prepared by homogeneous hydrolysis, exhibited a highly anisotropic morphology composed of elongated rod-like and flower-like aggregates. CeO_2_2, obtained by oxalate precipitation, consisted mainly of irregularly shaped agglomerates with plate-like subunits. In contrast, CeO_2_3, synthesized by precipitation with ammonium carbonate, showed more open lamellar/flake-like morphology, with thin plate-like structures and exposed edges. CeO_2_4, prepared by solution combustion synthesis, displayed a finely dispersed granular morphology composed of small, quasi-spherical

particles forming porous aggregates. The annealed commercial sample, CeO_2_5, consisted of larger agglomerated particles, most likely due to thermally induced sintering, whereas the amorphous commercial CeO_2_6 showed strongly agglomerated, poorly defined particulate morphology.

The EDS analysis in all samples confirmed the presence of cerium and oxygen atoms only (results not shown).

The Raman spectra of CeO_2_2 sample (crystalline) and CeO_2_6 sample (amorphous) are given in Figure 6.

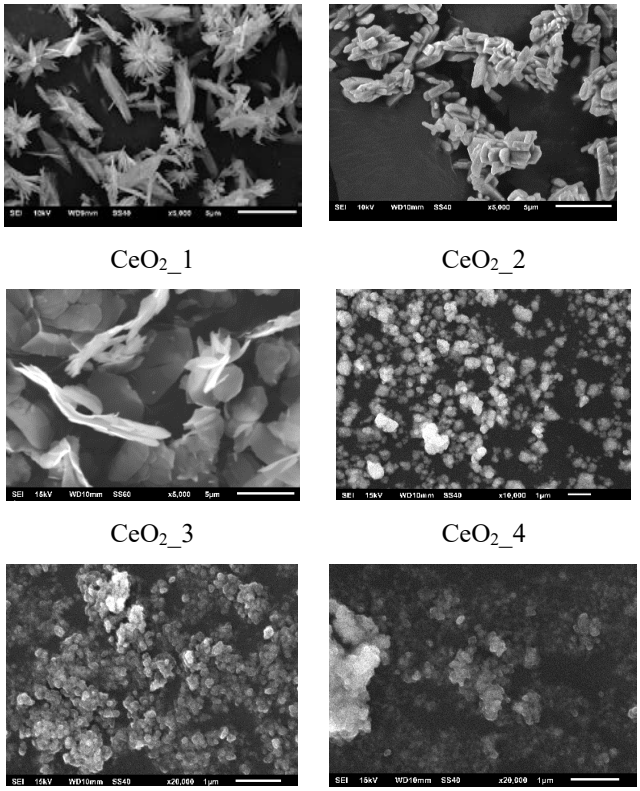


Figure 5. The SEM images of the CeO_2 samples under magnification of 5000x-20000x.

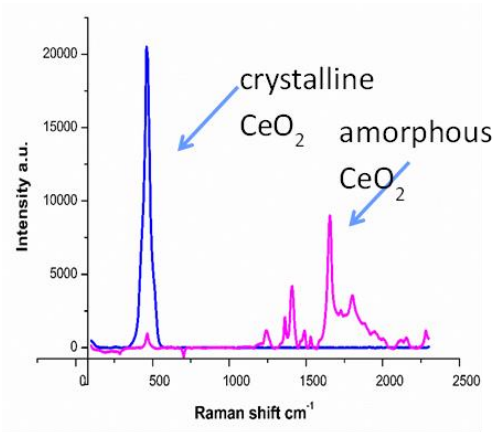


Figure 6. The Raman spectra of CeO_2_2 sample (crystalline) and CeO_2_6 sample (amorphous).

Raman spectroscopy was used to compare the structural ordering of selected CeO_2 samples. The crystalline CeO_2_2 sample exhibited a strong and sharp band at approximately 460–465 cm^{-1}, corresponding to the F2g mode of fluorite-type CeO_2, confirming the formation of a well-crystallized ceria phase. In contrast, the CeO_2_6 sample showed no dominant sharp F2g band, but rather a broadened and more complex spectral profile, indicating the absence of long-range crystalline order and confirming its amorphous or poorly crystalline character.

The pronounced spectral differences between these two samples demonstrate the strong influence of synthetic history and thermal treatment on the structural organization of CeO_2 nanoparticles.

Table 3. The specific surface area of the selected CeO_2 samples

	Sample		
	CeO2_3	**CeO2_5**	**CeO2_6**
Slope	30.8528	71.6628	69.0467
Intercept	0.274273	0.884697	1.12907
Correl. coeff.	0.999949	0.999857	0.999951
C constant	113.489	82.0026	62.1533
Surface area	111.881 m^2/g	48.003 m^2/g	49.626 m^2/g

In the Table 3, the specific surface area obtained by N_2 adsorption isotherms fitted by BET method are given. Nitrogen adsorption measurements revealed pronounced differences in the specific surface area of the selected CeO_2 samples. The highest BET surface area was obtained for CeO_2_3, synthesized by precipitation with ammonium carbonate, reaching 111.9 $m^2\ g^{-1}$. This value is more than two times higher than those measured for CeO_2_5 and CeO_2_6, which exhibited specific surface areas of 48.0 $m^2\ g^{-1}$ and 49.6 $m^2\ g^{-1}$, respectively. The high correlation coefficients of the BET plots confirmed the reliability of the linear fitting in the selected pressure range. The markedly larger surface area of CeO_2_3 is consistent with its open flake-like morphology observed by SEM and may contribute to the higher availability of surface-active sites for HD degradation.

3.3. The HD Degradation experiments

The removal/degradation profiles of HD over the investigated CeO_2 samples are presented in Figure 7. They clearly demonstrate that the catalytic performance strongly depends on the synthetic route. Among all samples, CeO_2_3 showed the highest degradation efficiency, reducing the relative HD concentration to approximately 0.16 after 70 min. A pronounced decrease was already observed during the first 20 min, indicating rapid interaction of HD with the surface-active sites. This superior performance is in good agreement with the SEM observations, where CeO_2_3 exhibited open lamellar/flake-like morphology with exposed edges, and with BET analysis, which showed the highest specific surface area for this sample, 111.9 $m^2\ g^{-1}$. Such morphology and high surface area may provide a larger number of accessible adsorption and reaction sites for HD degradation. CeO_2_4, obtained by solution combustion synthesis, also exhibited relatively high degradation efficiency, reaching a final relative HD concentration of approximately 0.34. Its activity may be associated with the

fine granular morphology and porous agglomerate structure typically formed during combustion synthesis. These features may favor the formation of defect-rich surfaces and facilitate the accessibility of HD molecules to catalytically active sites.

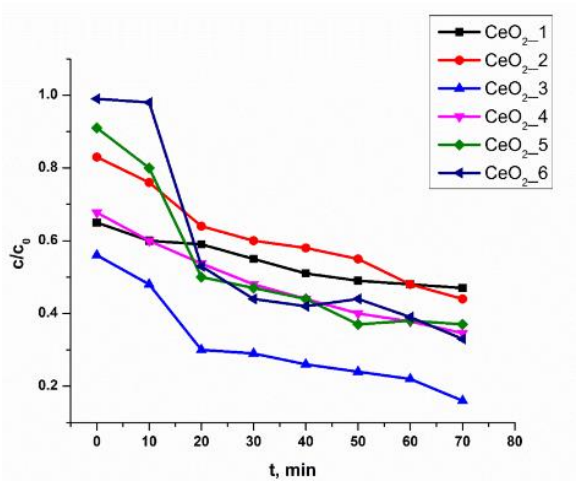


Figure 7. The HD removal over CeO_2 samples

In contrast, CeO_2_1 and CeO_2_2 showed lower degradation efficiency, despite their clearly developed morphologies. This suggests that anisotropic or crystalline morphology alone is not sufficient for high catalytic activity if the accessible surface area and density of reactive surface defects are not optimal. The comparison between CeO_2_2 and CeO_2_6 further indicates that crystallinity alone does not govern HD degradation. Raman spectroscopy confirmed that CeO_2_2 is crystalline, showing the characteristic fluorite CeO_2 band, while CeO_2_6 is amorphous or poorly crystalline. Nevertheless, CeO_2_6 showed considerable HD removal, especially after the first 20 min, despite its lower specific surface area of about 49.6 $m^2\ g^{-1}$ compared with CeO_2_3. This behavior may be related to the higher degree of structural disorder and defect concentration in amorphous CeO_2. However, its strongly agglomerated morphology probably limits the accessibility of these active sites, which may explain why it does not reach the performance of CeO_2_3. In order to obtain full degradation data with the posibility for the kinetic modelling and estimation which part of the HD removal includes adsorption and which is catalytic degradation, additional experiments should be performed with additional time points between 0 and 20 minutes.

4. CONCLUSONS

Overall, the results indicate that HD removal over CeO_2 nanoparticles is controlled by a combination of factors, including specific surface area, morphology, crystallinity, structural disorder, and probably the concentration of oxygen vacancies and Ce^{3+} surface sites. The high activity of CeO_2_3 appears to arise from the favorable combination of high surface area and open flake-like morphology, whereas the activity of CeO_2_4 may be related to its porous, combustion-derived, defect-rich structure. Therefore, the catalytic behavior cannot be explained solely by crystallinity or surface area, but rather by the accessibility and nature of surface-active sites.

Further research will encompass the incorporation of the most effective CeO_2 nanoparticles in the electrospun nanofibers of various polymers, as well as their application onto various substrates intended for CBRN protection, so the further work will consider the possibility of the scale-up of their application and use.

Acknowledgements

This work was supported by the Ministry of Science, Technological development and Innovations of the Republic of Serbia, Contract No. 451-03-34/2026-03/200325.

References

[1] E. M. Lucas and K. J. Klabunde, “Nanocrystals as destructive absorbants for mimcs of chemical warfare agents,” *Nanostructured Materials*, vol. 12, no. 1, pp. 179–182, 1999, doi: https://doi.org/10.1016/S0965-9773(99)00093-8.

[2] A. Khaleel, W. Li, and K. J. Klabunde, “Nanocrystals as stoichiometric reagents with unique surface chemistry. New adsorbents for air purification,” *Nanostructured Materials*, vol. 12, no. 1, pp. 463–466, 1999, doi: https://doi.org/10.1016/S0965-9773(99)00159-2.

[3] V. Štengl, T. M. Grygar, F. Opluštil, and T. Němec, “Ge4+ doped TiO2 for stoichiometric degradation of warfare agents,” *J. Hazard. Mater.*, vol. 227–228, pp. 62–67, 2012, doi: https://doi.org/10.1016/j.jhazmat.2012.05.007.

[4] V. Štengl *et al.*, “Zirconium doped nano-dispersed oxides of Fe, Al and Zn for destruction of warfare agents,” *Mater. Charact.*, vol. 61, no. 11, pp. 1080–1088, 2010, doi: https://doi.org/10.1016/j.matchar.2010.06.021.

[5] K. Ghabili, P. S. Agutter, M. Ghanei, K. Ansarin, Y. Panahi, and M. M. Shoja, “Sulfur mustard toxicity: History, chemistry, pharmacokinetics, and pharmacodynamics,” *Crit. Rev. Toxicol.*, vol. 41, no. 5, pp. 384–403, May 2011, doi: 10.3109/10408444.2010.541224.

[6] Gary S Groenewold, “Degradation kinetics of VX,” *Main Group Chemistry*, vol. 9, no. 3–4, pp. 221–244, Nov. 2010, doi: 10.3233/MGC-2010-0037.

[7] K. Otsuka, T. Ushiyama, and I. Yamanaka, “Partial Oxidation of Methane Using the Redox of Cerium Oxide,” *Chem. Lett.*, vol. 22, no. 9, pp. 1517–1520, Sep. 1993, doi: 10.1246/cl.1993.1517.

[8] S. Park, J. M. Vohs, and R. J. Gorte, “Direct oxidation of hydrocarbons in a solid-oxide fuel cell,” *Nature*, vol. 404, no. 6775, pp. 265–267, 2000, doi: 10.1038/35005040.

[9] V. Baldim, F. Bedioui, N. Mignet, I. Margaill, and J.-F. Berret, “The enzyme-like catalytic activity of cerium oxide nanoparticles and its dependency on Ce3+ surface area concentration,” *Nanoscale*, vol. 10, no. 15, pp. 6971–6980, Apr. 2018, doi: 10.1039/c8nr00325d.

[10] Y. Yang *et al.*, “Redox enzyme-mimicking activities of CeO2 nanostructures: Intrinsic influence of exposed facets,” *Sci. Rep.*, vol. 6, no. 1, p. 35344, 2016, doi: 10.1038/srep35344.